Ultrasonics Sonochemistry 88 (2022) 106068

Contents lists available at ScienceDirect

Ultrasonics Sonochemistry

journal homepage: www.elsevier.com/locate/ultson

Generation of subharmonics in acoustic resonators containing bubbly liquids: A numerical study of the excitation threshold and hysteretic behavior

María Teresa Tejedor Sastre [a], Olivier Louisnard [b], Christian Vanhille [a,*]

[a] NANLA, Universidad Rey Juan Carlos, Tulipán s/n 28933 Móstoles, Madrid, Spain
[b] Centre Rapsodee, UMR Centre National de la Recherche Scientifique 5302, IMT Mines Albi 81013 Albi CT, France

ARTICLE INFO

Keywords:
Bubbly liquids
Nonlinear acoustics
Subharmonics
Hysteresis

ABSTRACT

In this paper we study the generation and behavior of subharmonics in a bubbly liquid confined in an acoustic resonator, through numerical simulations carried out at finite-amplitude acoustic pressure. Several configurations in terms of resonator length and driving frequency are considered here. Our results show that these frequency components, created from a higher-frequency signal at the source (ultrasound), are due to the nonlinearity of the medium at high acoustic-pressure amplitude and to the configuration of the resonator (geometry and boundaries). We also show that they have an amplitude-threshold dependence, which is in concordance with the literature. The response of these subharmonics to different sequences of pressure amplitudes also reveals the hysteretic nature of the bubbly liquid.

1. Introduction

Ultrasound are commonly used in many sectors, such as industry and medicine [1]. In particular, ultrasonography is one of the most widely used diagnostic techniques, mainly because of its non-invasive nature, low cost and wide availability. This method is based on the reception of the waves reflected by the interfaces between different media within the volume to be evaluated, and takes advantage of the different propagation speeds to create an image.

When the difference between the propagation speed of the media is not very pronounced, strategies must be used to increase this difference and obtain sharper images. The main technique is the use of contrast agents, introducing a liquid with gas microbubbles into the bloodstream [2]. The presence of gas makes the speeds very different and, therefore, the quality of the image is hugely enhanced. In addition, because of the presence of bubbles, the media become highly nonlinear, causing other very interesting effects for diagnostics, such as the generation of new frequencies, harmonics and subharmonics [3,4].

The use of harmonics to obtain higher image quality, due to their better spatial resolution, is not very suitable with the control of the process because they can be caused by both bubbles and tissues [5]. However, subharmonics are more appropriate, because their existence is almost exclusively due to bubbles, and thus allows the control of the spot at which the user wants these new frequency components. The use of subharmonics to generate images reduces the processing and filtering of the signal obtained at the receiver [6,7].

A deep knowledge about the behavior and generation of subharmonics is a key factor to their use in ultrasound diagnostics. An important characteristic of subharmonics is their abrupt appearance when control parameters are varied. There is a threshold beyond which they are suddenly generated, as it has been studied for an uncoated bubble [8–12] and for a coated bubble [13–16]. All these works study the dynamics of a bubble excited by a linear continuous pressure source, but they do not consider the nonlinear retroaction of the bubble vibrations on the acoustic field.

In this work we consider the simplified case of an homogeneous distribution of uncoated bubbles in a liquid contained in a one-dimension rigid-walled resonator. Besides its theoretical interest for the knowledge about the behavior of nonlinear ultrasound in bubbly liquids, the analysis proposed here in this configuration might be helpful for diagnosis purpose, since when contrast agents are used, ultrasound can interact with structures of different dimensions, or be confined in a bubble layer or a bubble cloud, which can be resonant and lead to the generation of subharmonics. This study could also be useful in the sonochemistry framework to generate subharmonics in a resonant sonoreactor, which are acoustic waves of lower frequencies with lower

* Corresponding author.
E-mail address: christian.vanhille@urjc.es (C. Vanhille).

https://doi.org/10.1016/j.ultsonch.2022.106068
Received 7 April 2022; Received in revised form 25 May 2022; Accepted 13 June 2022
Available online 17 June 2022

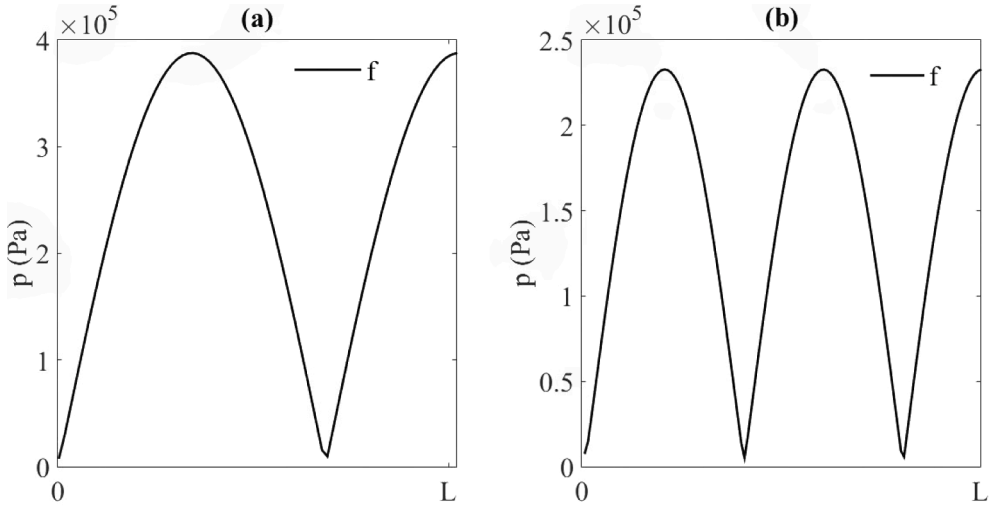

Fig. 1. Pressure amplitude distribution of frequency components in the cavity with $p_s = 12\text{kPa}, f = 300\text{kHz}$. $L = 3\lambda/4$ (a), and $L = 5\lambda/4$ (b).

attenuation.

We study the interaction between the acoustic field, modeled by the wave equation accounting for the bubbles, and the bubble vibrations, modeled by a Taylor-expanded Rayleigh Plesset equation, recalled in Section 2 and solved by means of an appropriate numerical model [17]. The rigid-wall condition is appropriate for generating subharmonics in a highly nonlinear bubbly liquid medium (see the paragraph right below Eq. (5)), as shown in [18]. The results obtained here indicate which type of resonator, in terms of geometrical aspects (length), is more convenient to generate subharmonics, in Section 3.1, and show that their nature is clearly nonlinear, in Sections 3.2.1 and 3.3.1. In Sections 3.2.2 and 3.3.2 the above-mentioned threshold is observed. In Section 3.4 the hysteretical nature of the bubbly liquid is demonstrated through the behavior of subharmonics when the pressure amplitude is either increased or decreased gradually. Section 4 gives the conclusions of this work.

2. Material and methods

We consider an ultrasonic field in a one-dimensional cavity of length L, filled with a bubbly liquid. We suppose an homogeneous distribution of spherical gas bubbles of the same size in the liquid. The initial bubble radius, R_{0g}, is assumed small compared to the wavelength of the acoustic field, λ. We study the nonlinear interaction of acoustic waves and bubble vibrations, which is modeled by a partial differential equations system [19–21]:

$$p_{xx} - p_{tt}/c_{0l}^2 = -\rho_{0l} N_g v_{tt},\ (x,t) \in (0,L) \times (0,T_l), \tag{1}$$

$$v_{tt} + \delta\omega_{0g} v_t + \omega_{0g}^2 v + \eta p = av^2 + b\left(2vv_{tt} + (v_t)^2\right),\ (x,t) \in [0,L] \times (0,T_l), \tag{2}$$

where $p(x,t)$ is the acoustic pressure and $v(x,t) = V(x,t) - v_{0g}$ is the bubble volume variation, x is the one-dimensional space coordinate, t is the time, T_l is the last instant of the study, $v_{0g} = \frac{4}{3}\pi R_{0g}^3$ is the initial volume of the bubbles, and $V(x,t)$ is the instantaneous volume of a bubble located at position x. In Eq. (1) (wave equation accounting for the bubbles), c_{0l} and ρ_{0l} are the sound speed and the density at the equilibrium state of the liquid, and N_g is the bubble density in the liquid. In Eq. (2) (Rayleight-Plesset equation), $\delta = 4\nu_l/\omega_{0g}R_{0g}^2$ is the viscous damping coefficient of the bubbly fluid, in which ν_l is the cinematic viscosity of the liquid, $\omega_{0g} = 2\pi f_{0g} = \sqrt{3\gamma_g p_{0g}/\rho_{0l}R_{0g}^2}$ is the isentropic resonance frequency of the bubbles, in which γ_g is the specific heats ratio of the gas, $p_{0g} = \rho_{0g}c_{0g}^2/\gamma_g$ is its atmospheric pressure, ρ_{0g} and c_{0g} are the density and sound speed at the equilibrium state of the gas. The other parameters are $\eta = 4\pi R_{0g}/\rho_{0l}, a = (\gamma_g + 1)\omega_{0g}^2/2v_{0g}$ and $b = 1/6v_{0g}$.

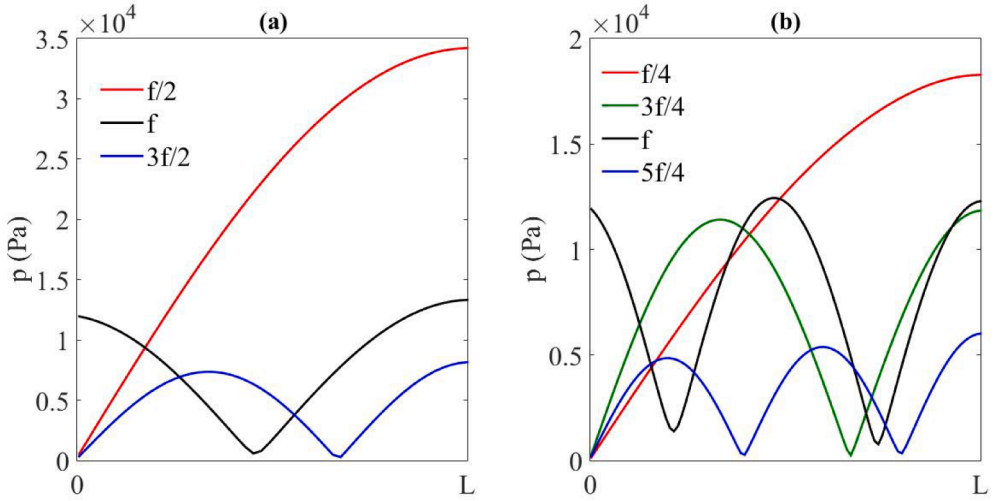

Fig. 2. Pressure amplitude distribution of frequency components in the cavity with $p_s = 12\text{kPa}, f = 300\text{kHz}$. $L = \lambda/2$ (a), and $L = \lambda$ (b).

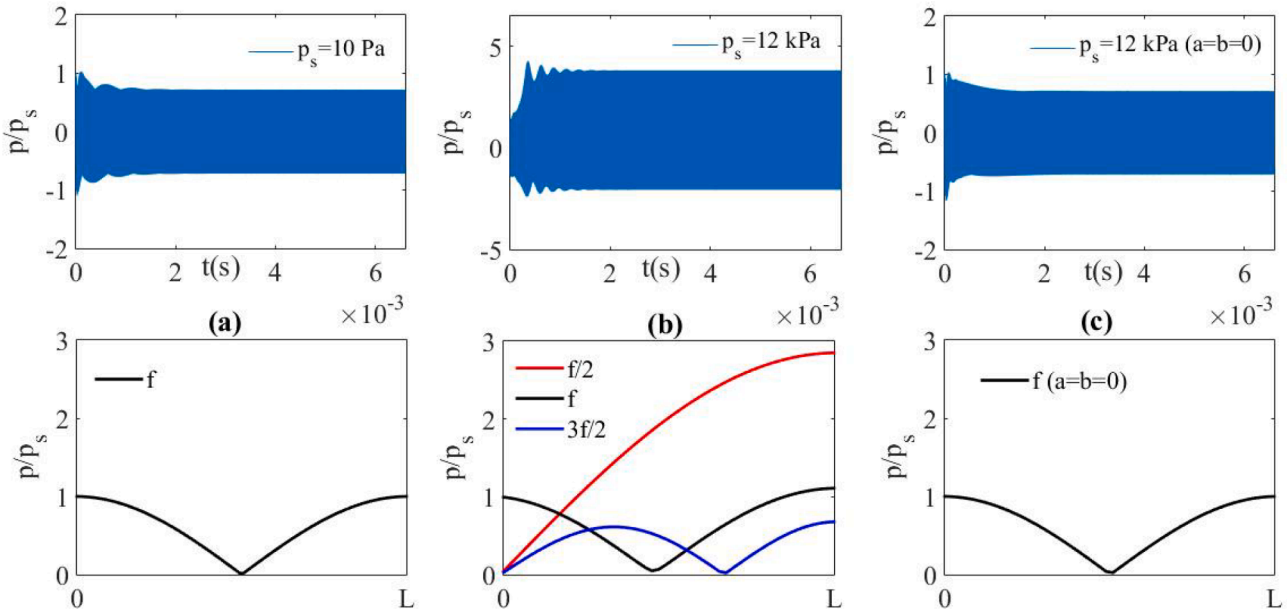

Fig. 3. Dimensionless pressure waveform and at the 3/4-length point of the cavity (top) and dimensionless pressure amplitude distribution of frequency components in the cavity (bottom) of length $L = \lambda/2$ with $f = 300$kHz during $T_l = 2000\ T$. Low amplitude $p_s = 10Pa$ (a), high amplitude $p_s = 12$kPa (b), and $p_s = 12$kPa without nonlinear terms in Eq. (2) (c).

Subscripts combining t and x denote partial derivatives.

Eqs. (1) and (2) are complemented with the following initial conditions:

$$p(x,0) = 0,\ v(x,0) = 0,\ p_t(x,0) = 0,\ v_t(x,0) = 0,\ \ x \in [0,L]. \tag{3}$$

Moreover, the cavity is excited by a time-dependent pressure source $s(t)$ of amplitude p_s and frequency $\omega = 2\pi f$ located at $x = 0$:

$$p(0,t) = s(t) = p_s \sin(\omega t),\ \ t \in [0,T_l], \tag{4}$$

and we assume a rigid-wall boundary condition at $x = L$:

$$p_x(L,t) = 0,\ \ \ t \in [0,T_l]. \tag{5}$$

This model assumes that bubbles are the only source of attenuation, dispersion, and nonlinearity in the fluid, they are monodisperse and oscillate at their first radial mode, and surface tension is neglected. The translational motion of the bubbles relative to the liquid, under Bjerknes, buoyancy, viscous drag and added-mass forces is not considered in this work [20,22].

This differential system, Eqs. (1)–(5), is solved using the numerical model developed in [17]. This tool is based on the finite-volume method in the space dimension and the finite-difference method in the time domain. In Section 3, 100 finite volumes per wavelength and 400 time points per period of f are used.

3. Results

The objective of this section is to study the generation of subharmonics from a single frequency by means of the model presented in Section 2. The following data for the bubbly liquid are set into the model: $c_{0l} = 1500\text{ms}^{-1}, \rho_{0l} = 1000\text{kg m}^{-3}$, and $\nu_l = 1.43 \times 10^{-6}\text{m}^2 s^{-1}$ for the liquid (water) and $c_{0g} = 340\text{ms}^{-1}, \rho_{0g} = 1.29\text{kg m}^{-3}$, and $\gamma_g = 1.4$ for the gas (air). We use bubbles of radius $R_{0g} = 2.5\mu$m (resonance frequency $f_{0g} = 1.35$MHz), and the bubble density is $N_g = 5 \times 10^{11}\text{m}^{-3}$. In the following, the final time of the simulations, T_l, is high enough to guarantee that the steady regime is reached in the resonator, i.e., $T_l = 2000\ T$ in Sections 3.1 (Figs. 1a and 2a), 3.2 and 3.4.1, $T_l = 4000\ T$ in Sections 3.1 (Figs. 1b and 2b), 3.3 and 3.4.2. A Fast Fourier Transform (FFT) is applied to the last 100 T of the acoustic pressure signal to study the distribution of its frequency components.

3.1. Resonators of length $L = (2n+1)\lambda/4$ vs. $L = n\lambda/2$, $n = 1, 2$

In this section the source frequency is $f = 300$kHz ($f/f_{0g} = 0.223$) and the source amplitude is $p_s = 12$kPa. We use cavities of length $L = 3\lambda/4$ and $L = 5\lambda/4$ (Fig. 1) vs. $L = \lambda/2$ and $L = \lambda$ (Fig. 2)) to determine which type of resonator is the most convenient to generate low frequency components in the configuration given via Eqs. (1)–(5). As it can be seen, when the resonator length is $L = (2n+1)\lambda/4$ (Fig. 1), new frequencies do not appear, although the maximum amplitude of the fundamental f is very high in both cases, 38.8kPa and 23.3kPa (323% and 194% of p_s), respectively. However, when the length is $L = n\lambda/2$ (Fig. 2), low and high frequencies appear. When the resonator length is $L = \lambda/2$ (Fig. 2a), a low frequency $f/2$ (red line) with maximum amplitude 34.2kPa (285% of p_s) and a high frequency (among others less intense) of large amplitude $3f/2$ (blue line), with maximum amplitude 8.08kPa (68.2% of p_s), are generated. When the resonator length is $L = \lambda$ (Fig. 2b), two low frequencies appear, $f/4$ and $3f/4$ (red and green line, respectively) with maximum amplitudes 18.3kPa and 11.8kPa (125% and 98.4% of p_s), respectively. A high frequency, $5f/4$ (blue line) with maximum amplitude 5.98kPa (49.8% of p_s), is also generated. Therefore, the resonators used in the following sections will be chosen within the set $L = n\lambda/2$.

3.2. Resonator of length $L = \lambda/2$

3.2.1. Nonlinear behavior

In this section the origin of the generation of new low-frequency components is studied. Fig. 3 shows the dimensionless acoustic pressure waveform at the 3/4-length point of the cavity during the entire time of the study, $T_l = 2000\ T$, (top) obtained at a low source amplitude, $p_s = 10Pa$ (Fig. 3a), at a high source amplitude, $p_s = 12$kPa (Fig. 3b), and at the same high source amplitude, $p_s = 12$kPa, but by canceling the nonlinear contributions in the differential system, i.e., $a = b = 0$ in Eq. (2) (Fig. 3c). As it can be seen, when the amplitude is high and a, b are not null, the amplitude in the cavity increases considerably. The corresponding frequency decompositions are shown in Fig. 3 (bottom). At low

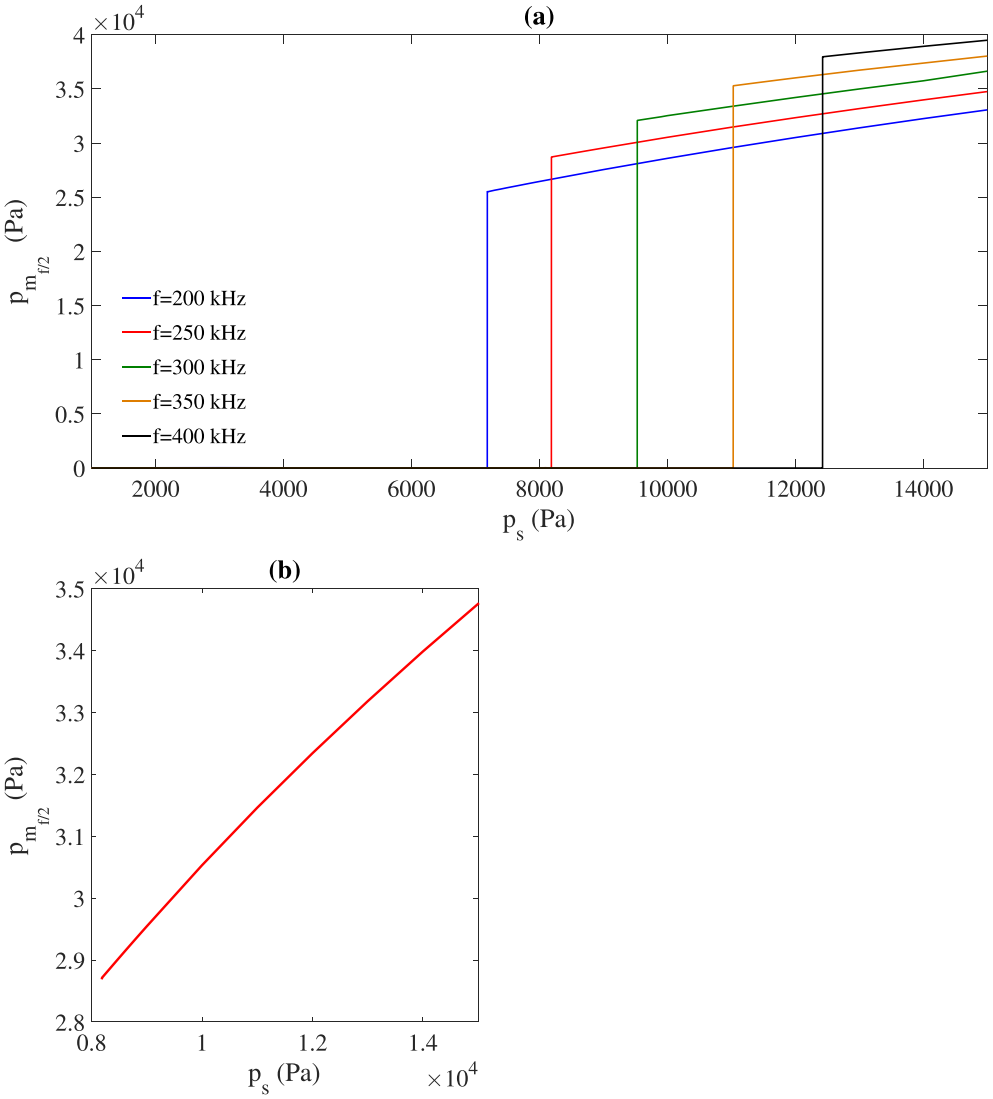

Fig. 4. Maximum amplitude of $f/2$-subharmonic $p_{m_{f/2}}$ in the cavity of length $L = \lambda/2$ vs. source amplitude p_s, (a) for several source frequencies: $f = 200$kHz (blue line), $f = 250$kHz (red line), $f = 300$kHz (green line), $f = 350$kHz (yellow line), $f = 400$kHz (black line), (b) once the threshold amplitude p_{th} is exceeded, for one frequency: $f = 250$kHz (red line).

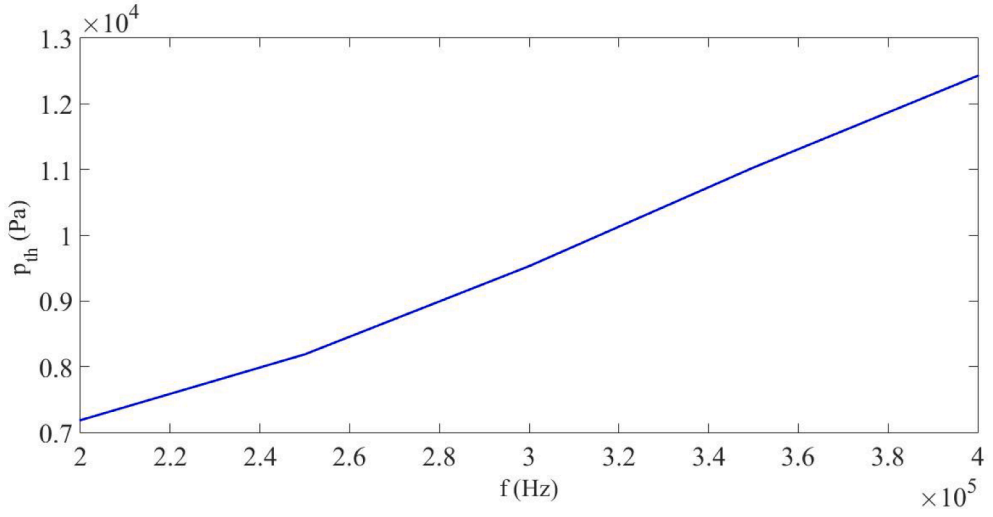

Fig. 5. Threshold amplitude p_{th} vs. source frequency f for $f/2$-subharmonic $p_{m_{f/2}}$ in the cavity of length $L = \lambda/2$.

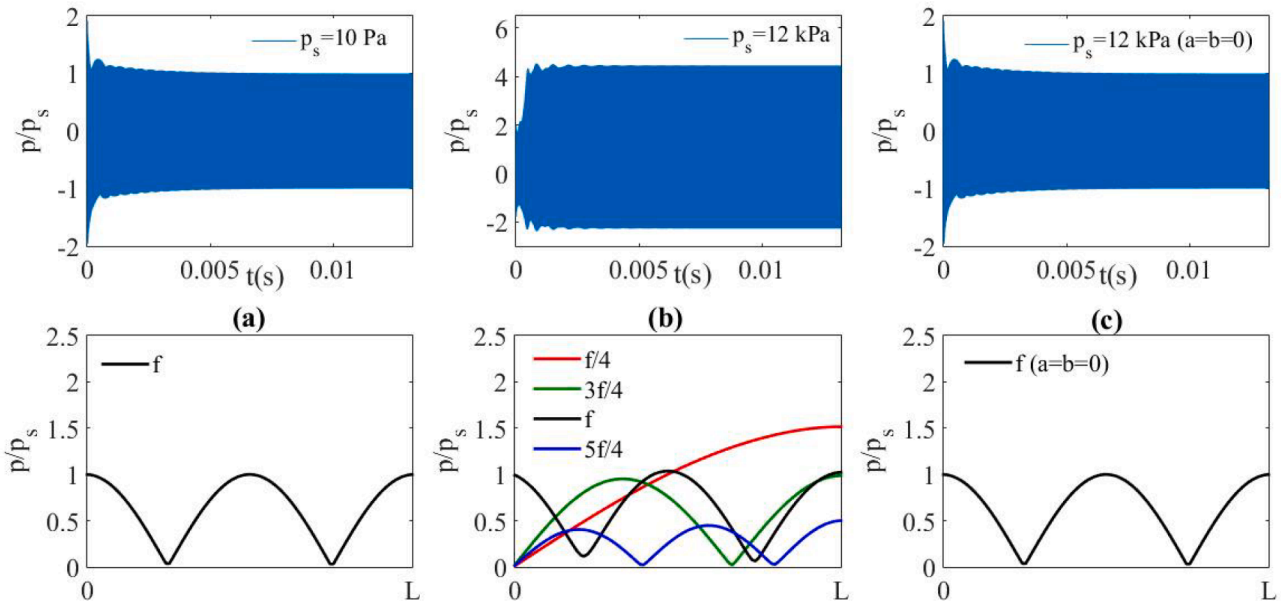

Fig. 6. Dimensionless pressure waveform and at the mid-point of the cavity (top) and dimensionless pressure amplitude distribution of frequency components in the cavity (bottom) of length $L = \lambda$ with $f = 300$kHz during $T_l = 4000\ T$. Low amplitude $p_s = 10$Pa (a), high amplitude $p_s = 12$kPa (b), and $p_s = 12$kPa without nonlinear terms in Eq. (2) (c).

source amplitude, $p_s = 10Pa$, there is only one component, the driving frequency f (Fig. 3a). At high amplitude, $p_s = 12$kPa, in addition to the source frequency, there are new frequency components (Fig. 3b). However, the cancellation of the nonlinear contributions in the differential system ($a = b = 0$ in Eq. (2)) prevents the new frequency components from being created, even at high source amplitude, $p_s = 12$kPa (Fig. 3c). These results clearly demonstrate that the generation of the new low-frequency components is a nonlinear effect.

3.2.2. *Study of subharmonic $f/2$ for several driving frequencies*

In this section we study the generation of the low-frequency component at $f/2$ as a function of the source amplitude p_s for several values of the driving frequency f ranging between 200 and 400kHz. To this purpose, the source amplitude p_s is raised from 1kPa to 15kPa, and we analyze whether the component $f/2$ appears or not by observing its maximum amplitude $p_{m_{f/2}}$.

As can be seen in Fig. 4a for several frequencies, when the amplitude p_s is low there is no $f/2$-component. However, above a threshold value p_{th}, the amplitude at $f/2$ increases suddenly and hugely up to 200% or 300% of p_s. Once this threshold is exceeded, the growth of the $f/2$-component, shown in Fig. 4b for $f = 250$kHz (which is representative of the five source frequencies studied here), seems to be linear for the five source frequencies studied here.

This behavior (existence of a excitation threshold, linear increase beyond the threshold) is the same for the five source frequencies studied here.

Moreover, the threshold value p_{th} increases with the driving frequency f, as evidenced in Fig. 5. This threshold amplitude seems to roughly follow a slight quadratic deviation from a linear behavior law vs. frequency.

3.3. *Resonator of length $L = \lambda$*

3.3.1. *Nonlinear behavior*

In this section the origin of the generation of new low-frequency components is studied. Fig. 6 shows the dimensionless acoustic pressure waveform at the mid-point of the cavity during the entire time of the study, $T_l = 4000\ T$, (top graphs) obtained at a low source amplitude, $p_s = 10$Pa (Fig. 6a), at high source amplitude, $p_s = 12$kPa (Fig. 6b), and at the same high source amplitude, $p_s = 12$kPa, but by canceling the nonlinear contributions in the differential system, i.e., $a = b = 0$ in Eq. (2) (Fig. 6c). As can be seen, when the amplitude is high and a, b are not null, the amplitude in the cavity increases considerably. The corresponding frequency decompositions are shown in Fig. 6 (bottom graphs). At low source amplitude, $p_s = 10$Pa, there is only one component, the source frequency f (Fig. 6a). At high amplitude, $p_s = 12$kPa, in addition to the driving frequency, there are new frequency components (Fig. 6b). However, the cancellation of the nonlinear contributions in the differential system ($a = b = 0$ in Eq. (2)) prevents the new frequency components from being created, even at high source amplitude, $p_s = 12$kPa (Fig. 6c). Like in Section 3.2.1, these results clearly demonstrate the nonlinear character of the generation of new low-frequency components in the resonator.

3.3.2. *Study of subharmonics $f/4$ and $3f/4$ for several driving frequencies*

In this section we study the generation of the low-frequency components at $f/4$ and $3f/4$ as a function of the source amplitude p_s for several values of the driving frequency f ranging between 200 and 350kHz. To this purpose, the source amplitude p_s is raised from 1kPa to 15kPa, and we analyze whether the $f/4$ and $3f/4$-components appear or not by observing their maximum amplitude, $p_{m_{f/4}}$ and $p_{m_{3f/4}}$, respectively.

As it can be seen in Fig. 7a for several frequencies, when the amplitude p_s is low no components at $f/4$ and $3f/4$ are observed. However, when the amplitude reaches a specific threshold value p_{th}, the amplitudes of $f/4$ and $3f/4$ subharmonics increase suddenly and abruptly up to 100% or 200% of p_s. The respective behaviors of $f/4$ and $3f/4$ subharmonics above this threshold, shown in Fig. 7b, left and right diagrams respectively, for $f = 250$kHz (which is representative of the four source frequencies studied here), differ in two aspects (compare solid and dashed curves in Fig. 7a): 1) the growth of the $f/4$-component amplitude seems to be linear and frequency-dependent (different slopes vs. frequency f), whereas the growth of the $3f/4$-component amplitude seems to follow a quadratic deviation from a linear behavior and almost frequency-independent; 2) the jump amplitude of the $f/4$-component at the threshold is an increasing function of frequency f, whereas the one of the $3f/4$-component is only slightly an increasing function of frequency f. Moreover, it must be noticed that the threshold amplitude is the same

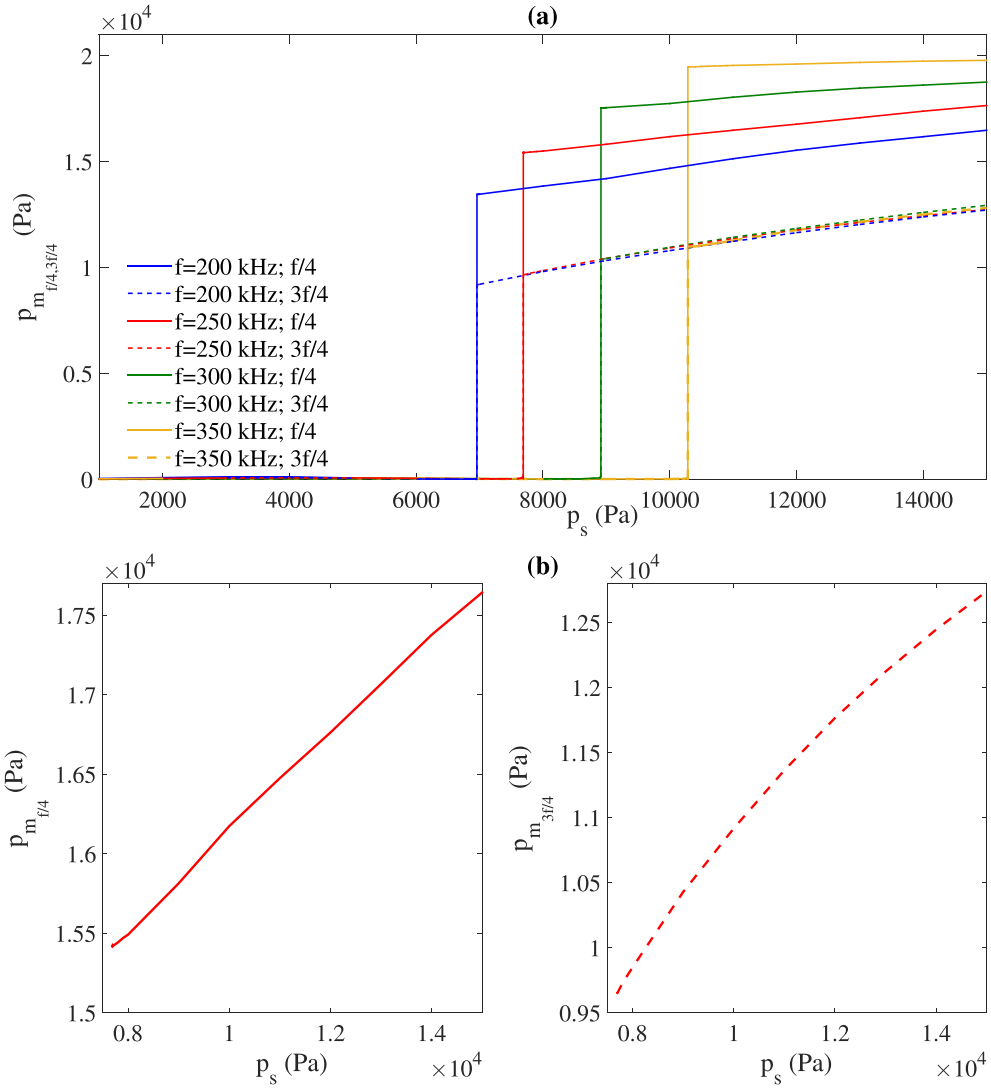

Fig. 7. Maximum amplitude of $f/4$ and $3f/4$-subharmonics, $p_{m_{f/4}}$ (solid lines) and $p_{m_{3f/4}}$ (dashed lines), in the cavity of length $L = \lambda$ vs. source amplitude p_s, (a) for several source frequencies: $f = 200$kHz (blue line), $f = 250$kHz (red line), $f = 300$kHz (green line), $f = 350$kHz (yellow line), (b) once the threshold amplitude p_{th} is exceeded, for one frequency: $f = 250$kHz (solid red line for $f/4$-subharmonic and dashed red line for $3f/4$-subharmonic).

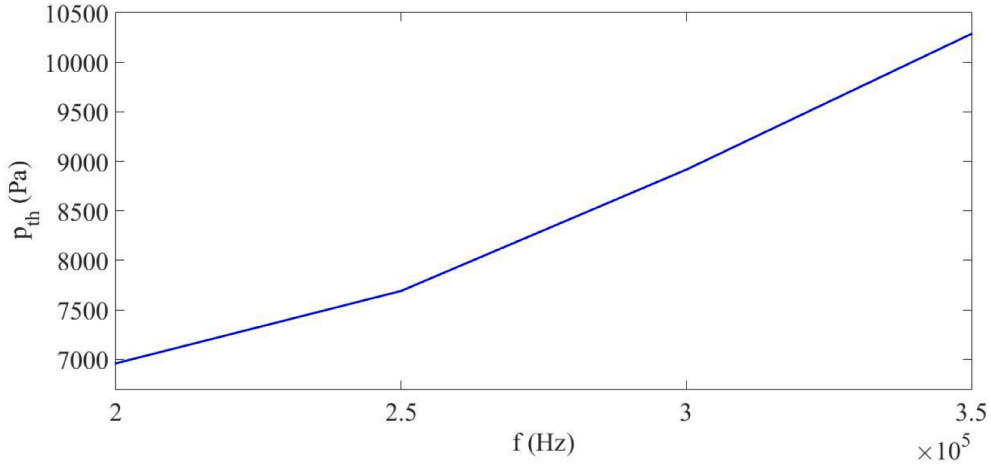

Fig. 8. Threshold amplitude p_{th} vs. source frequency f for both $f/4$ and $3f/4$-subharmonics, $p_{m_{f/4}}$ and $p_{m_{3f/4}}$, in the cavity of length $L = \lambda$.

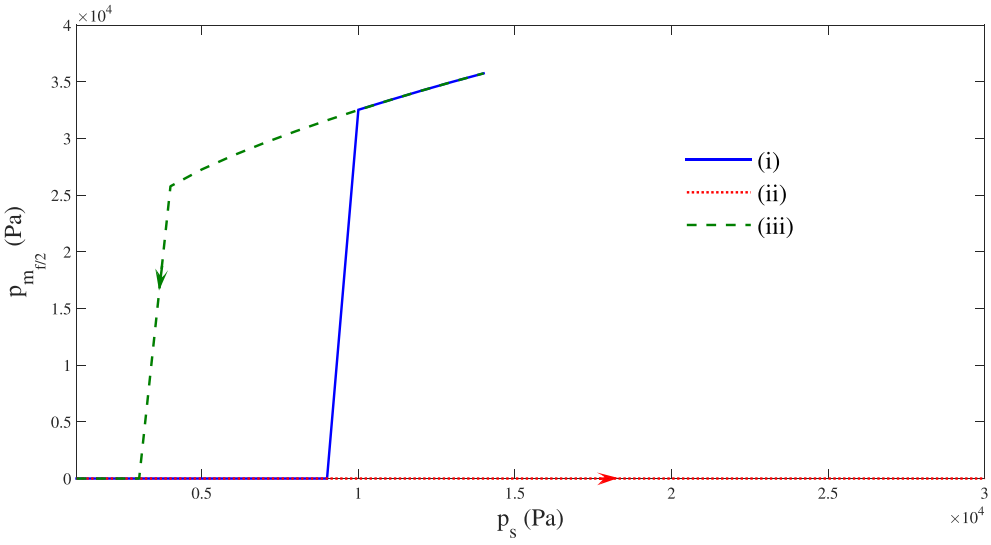

Fig. 9. Maximum amplitude of $f/2$-subharmonic $p_{m_{f/2}}$ for $f = 300$kHz in the cavity of length $L = \lambda/2$ when the source amplitude p_s is (i) increased starting from Eq. (3) (solid blue line), (ii) increased stepwise (dotted red line), and (iii) decreased stepwise (dashed green line).

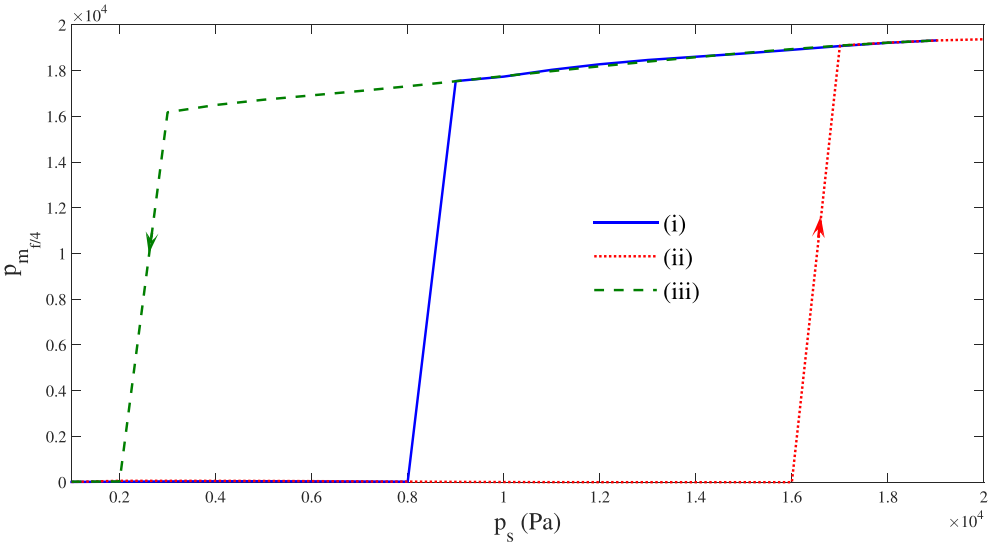

Fig. 10. Maximum amplitude of $f/4$-subharmonic $p_{m_{f/4}}$ for $f = 300$kHz in the cavity of length $L = \lambda$ when the source amplitude p_s is (i) increased starting from Eq. (3) (solid blue line), (ii) increased stepwise (dotted red line), and (iii) decreased stepwise (dashed green line).

for both frequency components. This suggests that the nonlinear subharmonic generation mechanism is strongly conditioned by the geometry of the resonator.

This behavior (existence of a excitation threshold, linear or slightly quadratic behavior beyond the threshold), observable for both subharmonics, is the same for the four source frequencies studied in this section.

Moreover, like in Section 3.2.2, the threshold value p_{th} increases with the driving frequency f, as evidenced in Fig. 8 for both subharmonics. Again this threshold amplitude seems to roughly follow a slight quadratic deviation from a linear behavior law.

3.4. Hysteretic character of subharmonic generation

In this section we study the hysteretic character of the subharmonic generation by refining the analysis of Sections 3.2 and 3.3, in the two cases $L = \lambda/2$ and $L = \lambda$, respectively. To this end, the pressure field in the cavity is computed twice, by stepwize increasing and stepwize decreasing the source amplitude p_s (using steps of 1kPa), the initial conditions considered for each step being the final conditions of the precedent one, instead of the generic initial conditions Eq. (3). We thus examine whether the direction in which the source amplitude is varied has an effect on the behavior of the subharmonics or not, and whether their appearance is hysteretic or not.

3.4.1. Resonator of length $L = \lambda/2$

Fig. 9 represents the maximum amplitude of the $f/2$-subharmonic ($p_{m_{f/2}}$) obtained at the driving frequency $f = 300$kHz in the resonator of length $L = \lambda/2$ (Sections 3.2) (i) when the source amplitude p_s is increased starting from Eq. (3) (solid blue line), (ii) when the amplitude is increased stepwise (dotted red line), and (iii) when the amplitude is decreased stepwise (dashed green line). It can be seen that the threshold for the subharmonic disappearance in Case (iii) ($p_{thd} = 3$kPa) is different from the appearance threshold in Case (i) ($p_{th} = 10$kPa). However, above these thresholds the behavior of $p_{m_{f/2}}$ remains the same in both cases. Case (ii) does not lead to the formation of the subharmonic, which would probably require higher amplitudes that cannot be handled by

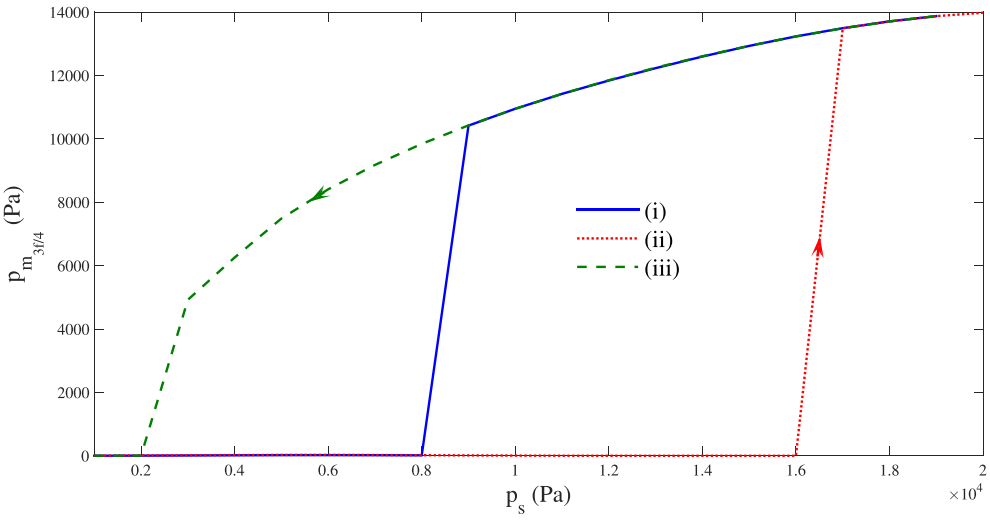

Fig. 11. Maximum amplitude of $3f/4$-subharmonic $p_{m_{3f/4}}$ for $f = 300$kHz in the cavity of length $L = \lambda$ when the source amplitude p_s is (i) increased starting from Eq. (3) (solid blue line), (ii) increased stepwise (dotted red line), and (iii) decreased stepwise (dashed green linee).

our model. Though Case (ii) is not conclusive, the comparison of Cases (i) and (iii) allows us to conclude about the existence of an hysteretic character of $f/2$-subharmonic generation.

3.4.2. Resonator of length $L = \lambda$

Figs. 10 and 11 represent the maximum amplitude of the $f/4$-subharmonic ($p_{m_{f/4}}$) and the $3f/4$-subharmonic ($p_{m_{3f/4}}$), respectively, for a driving frequency $f = 300$kHz in the resonator of length $L = \lambda$ (Sections 3.3) (i) when the source amplitude p_s is increased starting from Eq. (3) (solid blue line), (ii) when the amplitude is increased stepwise (dotted red line), and (iii) when the amplitude is decreased stepwise (dashed green line). It can be seen that the threshold for the disappearance of both subharmonics in Case (iii) ($p_{th} = 3$kPa) and the threshold for their appearance in Case (i) ($p_{th} = 9$kPa) and in Case (ii) ($p_{th} = 17$kPa) are different. These three thresholds have the same values for both $f/4$ and $3f/4$-subharmonics. However, above these thresholds the amplitudes $p_{m_{f/4}}$ and $p_{m_{3f/4}}$ remains the same in the three cases. The comparison of Cases (i), (ii), and (iii) allows us to conclude about the existence of an hysteretic character of $f/4$ and $3f/4$-subharmonics generation.

As seen before [23], a change in acoustic pressure amplitude modifies the characteristics of the bubbly medium (the average size of the bubbles, i.e., the void fraction in the liquid, is pressure amplitude dependent) and the resonance of the cavity containing it. Following this result, the threshold effect of a subharmonic is most likely due to the sudden match of the subharmonic frequency and the cavity resonance. The hysteretical behavior of this subharmonic may rely on the fact that the modifications of those characteristics of the medium are different depending on whether that pressure amplitude is raised or lowered. Further investigations are needed for a more comprehensive exploration of these points. They are part of our ongoing work.

4. Conclusions

We have carried out numerical experiments to study the generation of subharmonics in a bubbly liquid from a single-frequency ultrasonic driving signal in a one-dimensional resonator. The numerical simulations rely on a nonlinear mathematical model that couples the bubbles oscillations and the acoustic field. It has been shown via the model used here that the creation of subharmonics is a nonlinear effect and that the resonators that better suit this purpose in the boundary configuration assumed in this paper are those which length is a multiple of $L = \lambda/2$. The amplitude-threshold for the creation of subharmonics has been observed. The hysteretic nature of subharmonic generation in bubbly liquids has also been shown through the behavior of subharmonic components when different sequences of pressure amplitudes are applied at the source, which is the main point of this paper, since it has hardly been mentioned in the literature.

CRediT authorship contribution statement

María Teresa Tejedor Sastre: Conceptualization, Methodology, Software, Validation, Investigation, Data curation, Writing - original draft, Visualization. **Olivier Louisnard:** Conceptualization, Methodology, Validation, Writing - review & editing. **Christian Vanhille:** Conceptualization, Methodology, Software, Validation, Investigation, Data curation, Writing - original draft, Writing - review & editing, Supervision, Project administration, Funding acquisition.

Declaration of Competing Interest

The authors declare the following financial interests/personal relationships which may be considered as potential competing interests: Christian Vanhille reports financial support was provided by National Agency for Research (Agencia Estatal de Investigación, AEI), Ministry of Science and Innovation of Spain (Ministerio de Ciencia e Innovación), and the European Regional Development Fund (FEDER). Olivier Louisnard reports administrative support was provided by French Centre National de la Recherche Scientifique (CNRS).

Acknowledgements

This work is supported by the National Agency for Research (Agencia Estatal de Investigación, AEI), Ministry of Science and Innovation of Spain (Ministerio de Ciencia e Innovación), and the European Regional Development Fund (FEDER) [Grant No. DPI2017-84758-P]. One of us (OL) would also like to thank the French Centre National de la Recherche Scientifique (CNRS) for support via the cavitation research group (GDR CAVITATION).

References

[1] J. Gallego-Juárez, K. Graff, Power Ultrasonics: Applications of High-Intensity Ultrasound, Elsevier, 2014.
[2] J. Berry, P. Sidhu, Microbubble contrast-enhanced ultrasound in liver transplantation, Eur. Radiol. 14 (Suppl 8) (2004) 96–103.
[3] S. Kumar, C. Brennen, Nonlinear effects in the dynamics of clouds of bubbles, J. Acoust. Soc. Am. 89 (1991) 707–714.

[4] A. Eller, Subharmonic response of bubbles to underwater sound, J. Acoust. Soc. Am. 55 (1974) 871–873.
[5] T. Desser, R. Jeffrey, Tissue harmonic imaging tecniques: Physical principles and clinical aplications, Semin. Ultrasound CT MRI 22 (2001) 1–10.
[6] F. Forsberg, W. Shi, B. Goldberg, Subharmonic imaging of contrast agents, Ultrasonics 38 (1) (2000) 93–98.
[7] P. Shankar, P. Krishna, V. Newhouse, Advantages of subharmonic over second harmonic backscatter for contrast-to-tissue echo enhancement, Ultrasound Med. Biol. 24 (3) (1998) 395–399.
[8] A. Eller, H. Flynn, Generation of subharmonics of order one-half by bubbles in a sound field, J. Acoust. Soc. Am. 46 (1969) 722–727.
[9] W. Lauterborn, Numerical investigation of nonlinear oscillations of gas bubbles in liquids, J. Acoust. Soc. Am. 59 (1976) 283–293.
[10] Y. Fan, H. Li, D. Fuster, Optimal subharmonic emission of stable bubble oscillations in a tube, Phys. Rev. E 102 (2020), 013105.
[11] A. Sojahrood, R. Earl, M. Kolios, R. Karshafian, Investigation of the 1/2 order subharmonic emissions of the period-2 oscillations of an ultrasonically excited bubble, Phys. Lett. A 384 (23) (2020), 126446.
[12] A. Sojahrood, H. Haghi, N. Shirazi, R. Karshafian, M. Kolios, On the threshold of 1/2 order subharmonic emissions in the oscillations of ultrasonically excited bubbles, Ultrasonics 112 (2021), 106363.
[13] P. Shankar, P. Krishna, V. Newhouse, Subharmonic backscattering from ultrasound contrast agents, J. Acoust. Soc. Am. 106 (4) (1999) 2104–2110.
[14] A. Prosperetti, A general derivation of the subharmonic threshold for non-linear bubble oscillations, J. Acoust. Soc. Am. 133 (2013) 3719–3726.
[15] A. Katiyar, K. Sarkar, Excitation threshold for subharmonic generation from contrast microbubbles, J. Acoust. Soc. Am. 130 (2011) 3137–3147.
[16] A. Katiyar, K. Sarkar, Effects of encapsulation damping on the excitation threshold for subharmonic generation from contrast microbubbles, J. Acoust. Soc. Am. 132 (2012) 3576–3585.
[17] M.T. Sastre, C. Vanhille, A numerical model for the study of the difference frequency generated from nonlinear mixing of standing ultrasonic waves in bubbly liquids, Ultrason. Sonochem. 34 (2017) 881–888.
[18] O. Louisnard, Contribution à l'étude de la propagation des ultrasons en milieu cavitant. (French), Ph.D. Thesis Dissertation, École des Mines de Paris, 1998.
[19] F. Greiser, P. Choi, N. Enomoto, H. Harada, K. Okitsu, K. Yasui, Sonochemistry and the Acoustic Bubble, Elsevier, 2015.
[20] M. Hamilton, D. Blackstock, Nonlinear Acoustics, Academic Press, 1998.
[21] K. Naugolnykh, L. Ostrovsky, Nonlinear Wave Processes in Acoustics, Cambridge University Press, 1998.
[22] A. Doinikov, Bjerknes forces and translational bubble dynamics, Vol. Bubble and Particle Dynamics in Acoustic Fields: Modern Trends and Applications, Research Signpost, 2005.
[23] M.T. Sastre, C. Vanhille, Nonlinear resonance of cavities filled with bubbly liquids: A numerical study with application to the enhancement of the frequency mixing effect, Shock Vib. 2018 (2018) 1570508.